In-situ damage mechanism investigation and a prediction model for delamination with fibre bridging in composites

Yao, Liaojun; Liu, Jurui; Lyu, Zhangming; Alderliesten, R. C.; Hao, Cui; Ren, Chuanxi; Guo, Licheng

Important note
To cite this publication, please use the final published version (if applicable).
Please check the document version above.

In-situ damage mechanism investigation and a prediction model for delamination with fibre bridging in composites

Liaojun Yao [a,*], Jurui Liu [a], Zhangming Lyu [a], R.C. Alderliesten [b], Cui Hao [c], Chuanxi Ren [d], Licheng Guo [a]

[a] Department of Astronautics Science and Mechanics, Harbin Institute of Technology, Harbin, PR China
[b] Structural Integrity and Composites Group, Faculty of Aerospace Engineering, Delft University of Technology, the Netherlands
[c] School of Civil Aviation, Northwestern Polytechnical University, Suzhou, PR China
[d] Shi-Changxu Innovation Center for Advanced Materials, Institute of Metal Research, Chinese Academy of Sciences, Shenyang, PR China

A R T I C L E   I N F O

A B S T R A C T

Carbon-fibre reinforced composites are susceptible to delamination. Fibre bridging is an important shielding mechanism frequently observed in delamination. The presence of these bridging fibres can significantly increase interlaminar resistance, making it critical to represent this phenomenon for delamination characterization in composite laminates. To this end, in-situ SEM examinations were carried out to thoroughly explore damage mechanisms around delamination front as well as in bridging fibres. It was found that micro-cracks initiated at fibre–matrix interface can gradually develop and coalesce into micro-delaminations ahead of the main crack. The accumulation of these micro-delaminations can finally cause macro delamination propagation. The performance of bridging fibres can be summarized as three typical stages, i.e. bending, fibre–matrix peeling and final breakage with crack opening. Subsequently, theoretical discussions on bridging stress distribution were conducted in accordance with these bridging mechanism examinations, contributing to a new traction-separation constitutive to represent fibre bridging performance. A FEA prediction model was finally developed to characterize delamination behavior with fibre bridging. The simulation results can agree well with the experimental data in the entire delamination, demonstrating its effectiveness in fibre-bridged delamination representation. This study also demonstrated the importance of having in-depth understanding on fibre bridging mechanisms to appropriately represent bridging performance during delamination growth in composite laminates.

1. Introduction

Carbon fibre reinforced composites have been widely used in aerospace industry, because of their excellent mechanical properties and great weight-saving potential. However, it is evident that composite laminates are susceptible to delamination growth, a unique damage evolution occurring between neighbored layers for the lack of reinforcement through thickness direction. The initiation and propagation of this damage can cause stiffness/strength degradation, and may finally lead to catastrophic failure of a composite structure during its operating life. Accordingly, a large number of experimental and numerical studies have been conducted to explore

delamination behavior in composites [1–5].

In addition to interlaminar damage evolution around delamination front, significant bridging fibres, acting as a shielding mechanism in the wake of crack front, have been frequently observed and reported in delamination growth of composites [5–10]. Particularly, this toughening phenomenon occurs when one end of a fibre remains attached to one of the fracture surfaces, while the other end remains attached to the other surface. These bridging fibres therefore can form a loading path that bridges the crack. This performance can cause significant stress concentration alleviation and interlaminar resistance increase. It is therefore important to have reliable models to represent this phenomenon in delamination growth study.

Resistance curve (i.e. *R*-curve) expressed in terms of interlaminar resistance against crack propagation length $G_{IC}(a\text{-}a_0)$, and bridging law expressed in terms of bridging closure stress against crack opening displacement $\sigma_{br}(\delta)$ have been mostly employed to describe fibre bridging behavior in delamination growth [5,7,9,10]. It has been reported several times that the shape of *R*-curve is geometry dependent, making it not a material property [5,9,11]. As a result, the concept of bridging law has been increasingly used in fibre-bridged delamination growth studies [11–14]. Suo et al [15] initially proposed a J-integral approach to extract bridging law for delamination growth of composites. And the bridging stress can be determined via the derivative of interlaminar resistance G_{IC} with respect to crack opening displacement δ, see Eq.(1). This method has been frequently used by many people in bridging law determination [5,16–20]. However, one should keep in mind that the correlation between G_{IC} and δ should be determined as a prerequisite using Eq.(1) in the determination of bridging traction-separation law. And there is no consensus on the explicit formula of $G_{IC}(\delta)$ until now. Various functions indeed have been proposed to have $G_{IC}(\delta)$, but without any critical discussion on their validation [5,14,16–21]. Particularly, as discussed in literature [21], it is only a tool to make people conveniently determine the bridging law, but lack of solid connections with physical bridging mechanisms.

$$\sigma_{br}(\delta) = \frac{\partial G_{IC}(\delta)}{\partial \delta} \tag{1}$$

Instead of using the J-integral approach to determine the bridging law, Botsis et al [11,12,22,23] applied fibre Bragg gating sensor to monitor strain distribution in the vicinity of delamination front plane. They proposed an iterative method to determine the traction-separation stress in fibre bridging via minimizing the difference between experimental measurements (i.e. strains) and numerical predictions. These determined bridging closure stresses were subsequently implemented in a cohesive zone formulation to numerically represent fibre bridging behavior in delamination growth.

According to the previous studies [11–18,20–23], different traction-separation laws have been proposed to represent fibre bridging in delamination growth. It is true that people can use these bridging laws with different shapes to represent bridging behavior in the perspective of energy balance. However, there is still lack of physical understanding on this phenomenon, especially on the real bridging stress distribution. Particularly, as mentioned by Spearing et al [24] and Bao et al [25], different bridging mechanisms can cause difference in bridging stress distribution. Thus, the key questions arise as:

(1) What are the damage mechanisms in bridging fibres during delamination?

(2) What is the real traction-separation response in bridging fibres during delamination?

To solve these issues, both macro and in-situ experiments were conducted in the present study to explore delamination resistance, interlaminar damage mechanisms and bridging mechanisms of carbon fibre reinforced composites. Incorporating with a micromechanical model proposed in the literature [26], the traction-separation response in bridging fibres was theoretically discussed and identified, contributing to a trapezoid-nonlinear traction-separation law to capture the essential feature of bridging stress distribution. And a new delamination constitutive was finally proposed via superposition strategy to numerically simulate fibre-bridged delamination behavior in composite laminates.

2. Macro and in-situ SEM experiments

Both macro and in-situ experiments were conducted to explore delamination behavior and corresponding damage mechanisms in composite laminates. Particularly, the macro delamination tests were performed to determine the increase of interlaminar resistance with crack propagation because of fibre bridging. The in-situ SEM examinations were carried out to explore damage mechanisms both around delamination front and in bridging fibres.

2.1. Macro delamination experiments

The material applied here was carbon fibre/epoxy prepreg M30SC/DT120 (high strength and modulus carbon fibre/toughened thermosetting epoxy). Composite laminates were laid in the designed stacking sequence, i.e. $[0_{16}//0_{16}]$. A Teflon insert with 12.7 μm thickness was placed in the middle plane to introduce an initial delamination. Laminates were cured in the autoclave at a pressure of 6 bars and curing temperature of 120℃ for 90 min. After curing, the laminates were C-scanned for imperfections. Samples were taken from the areas where no imperfections were identified. Unidirectional double cantilever beam (DCB) specimens, $L = 200.0$ mm length by $B = 25.0$ mm width with thickness of $h = 5.0$ mm, were cut from the composite panel with a diamond-coated cutting machine. One side of each DCB specimen was coated with a thin layer of typewriter correction to enhance the visibility of delamination front during the tests. A strip of grid paper was pasted on the typewriter correction coated side to aid in measuring crack propagation length.

All quasi-static delamination tests were carried out on a 20kN tensile-compression Zwick machine at Delft Aerospace Structures and Materials Laboratory, as shown in Fig. 1. These tests were performed under displacement control with a constant applied rate of 1.0 mm/min. A computer controlled digital camera system with high resolution was employed to monitor the delamination propagation
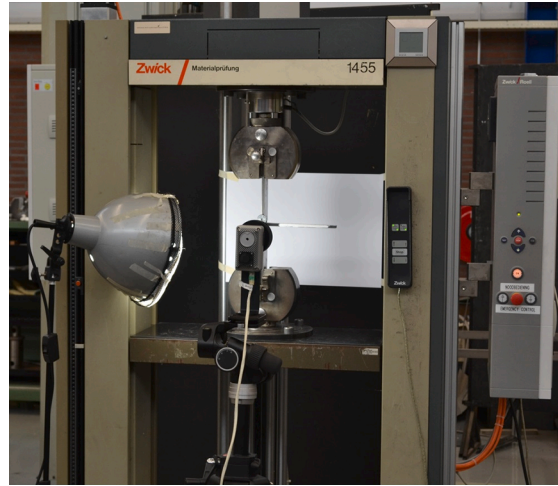
Fig. 1. Macro delamination experimental setup.

via automatically recording an image of the specimen edge every 5 s.

The Modified Compliance Calibration (MCC) method, see Eq.(2), recommended in the ASTM D5528 standard was employed to calculate the interlaminar resistance G_{IC} in quasi-static delamination tests, with the load, displacement and measured crack length information.

$$G = \frac{3P^2 C^{(2/3)}}{2A_1 Bh}$$

(2)

where P is the load; C is the compliance of the DCB specimen; A_1 is the slope of the curve in the graph where a/h is plotted against $C^{1/3}$.

2.2. In-situ SEM examination tests

Two kinds of in-situ SEM experiments were carefully conducted in the present study to explore damage mechanisms both around delamination front and in bridging fibres. Particularly, the in-situ samples, $L = 10.0$ mm length by $B = 3.0$ mm width with thickness of $h = 5.0$ mm, for micro damage examinations at crack front were cut from DCB specimens with a multidirectional interface, i.e. [(±45/0_{12}/∓45)//(±45/0_{12}/∓45)]. And two holes, with diameter of $d = 1.0$ mm, were machined on these samples at the pre-crack side for loading introduction during the in-situ experiments. Fig. 2(a) illustrates the configuration of in-situ experiments for damage evolution examinations around delamination front.

The reason why using multidirectional instead of unidirectional sample on crack front damage observations is to have clear examinations on micro damage initiation and propagation that occurs between reinforced carbon fibre and matrix, as it has been reported that micro-cracks initiated at fibre–matrix interface could play an important role in the failure of composite laminates [27]. However, if one use unidirectional in-situ sample, it is difficult to identify these micro-cracks at fibre–matrix interface as well as their accumulation during delamination growth, as the reinforced carbon fibres are parallel to crack propagation direction. According to our previous study [7], it was reported that the initial interlaminar resistance (excluding fibre bridging contribution) is almost the same for DCB specimens with unidirectional and multidirectional stacking sequence. As the initial delamination resistance mainly depends on damage evolution around crack front, one can therefore make a conclusion that damage propagation around crack front remains the same or at least similar for DCB specimens with unidirectional and multidirectional stacking sequence. In addition, according to our in-situ observations on fibre bridging performance in both unidirectional and multidirectional samples, the stacking sequence can only have effects on the significance of fibre bridging, i.e. the amount of bridging fibres generated at per unit area. However, no obvious difference was observed in the bridging failure mechanisms as we reported in the present manuscript.

Macro tested unidirectional DCB samples were polished in side with water mill polishing machine, in order to identify the crack tip location via microscope. The in-situ DCB specimens for fibre bridging mechanism examinations, with the same configuration (i.e. $L = 10.0$ mm length by $B = 3.0$ mm width with thickness of $h = 5.0$ mm), were cut from these tested unidirectional DCB specimens. These in-situ samples, typically containing a 3–5 mm crack propagation (i.e. a certain amount of bridging fibres), were adhesively bonded to a couple of well-designed hinges for load introduction during the micro examinations. Fig. 2(b) provides the configuration of these experiments for bridging mechanism examinations.

One side of each in-situ sample was carefully polished with the polishing machine. These appropriately polished samples were subsequently prepared with gold sputter-coating to avoid static charging during in-situ SEM examinations, due to the non-conductive natural of the composite material used in the present study.

The in-situ tests for examining damage evolution around delamination front were conducted on an in-situ SEM tensile system of the
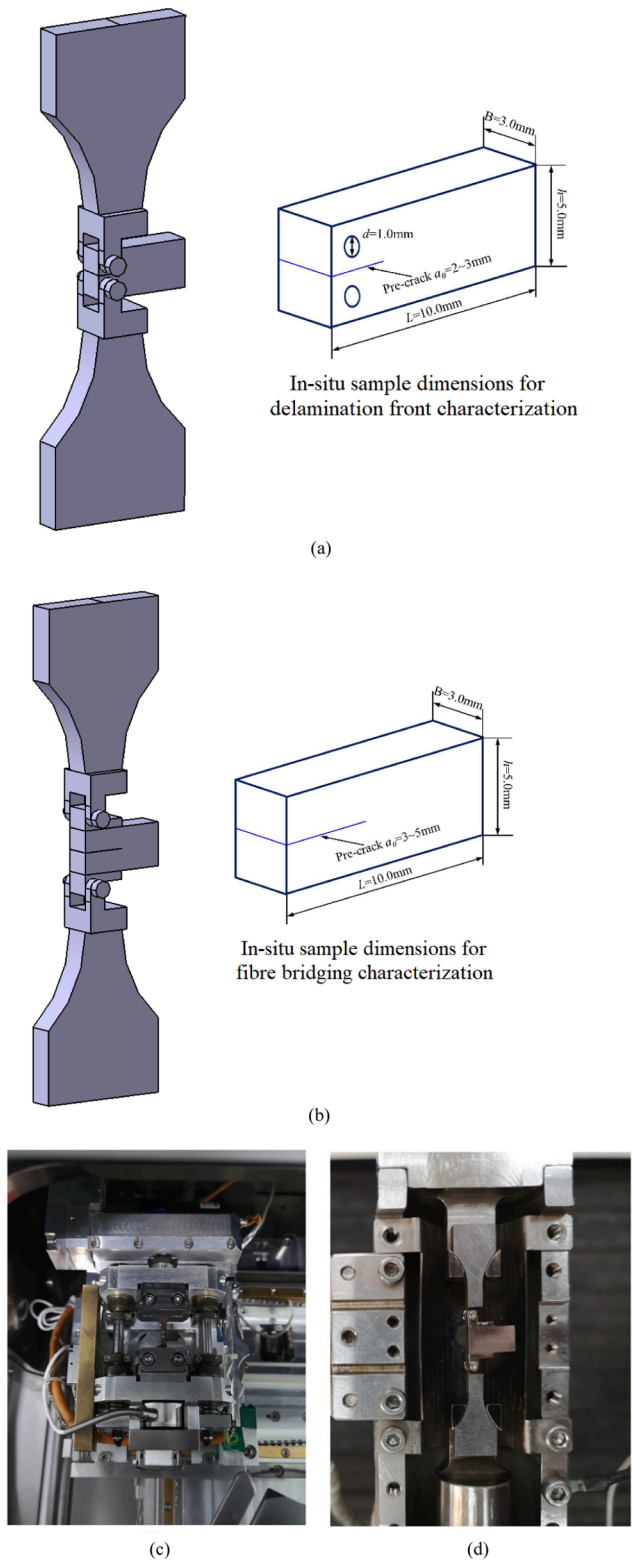
Fig. 2. In-situ SEM experimental setups (a) In-situ experimental configuration for delamination front observation; (b) In-situ experimental configuration for fibre bridging observation; (c) In-situ experimental setup for delamination front examination; (d) In-situ experimental setup for fibre bridging examination.
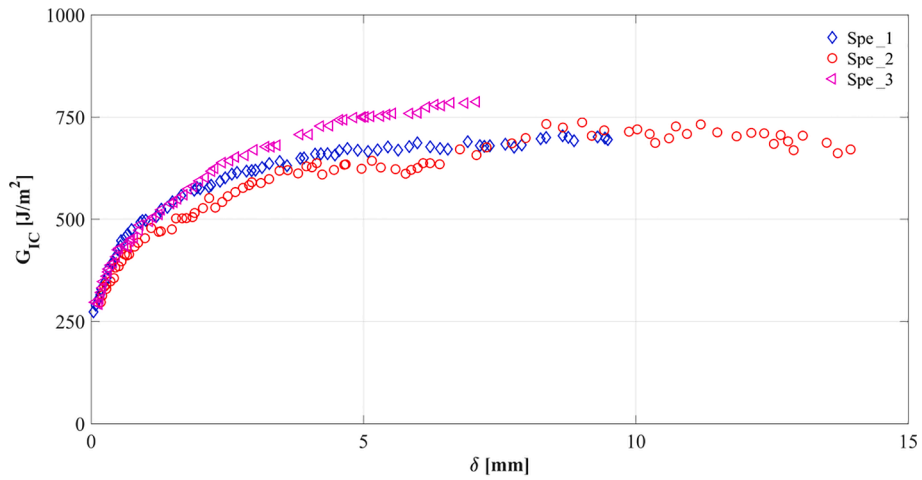
Fig. 3. Delamination resistance increase with crack opening.

Fig. 4. Fibre bridging in delamination growth of carbon fibre reinforced composites.
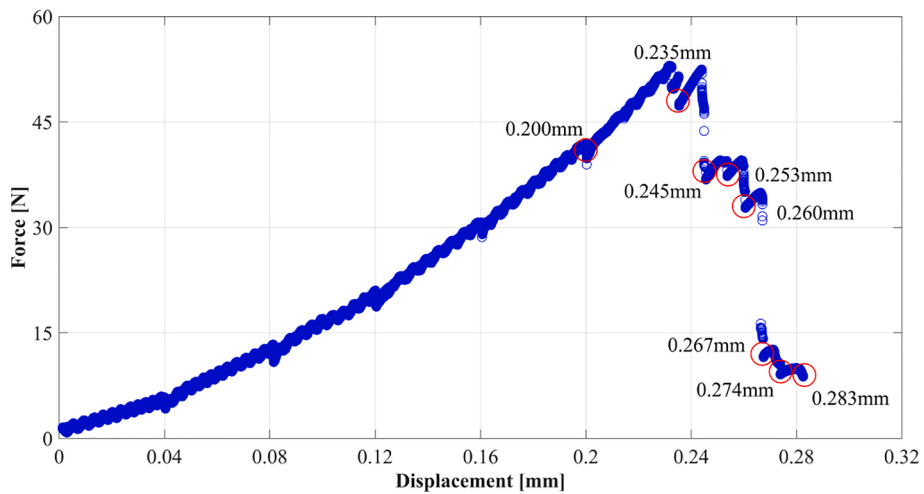
Fig. 5. Load-displacement response for in-situ experiments on delamination front.

Harbin Institute of Technology, which is assembled with in-situ tensile apparatus inside of a Helios NanoLab600i SEM, see Fig. 2(c). The in-situ fibre bridging examinations were conducted on another in-situ SEM tensile system of Institute of Metal Research, Chinese Academy of Sciences, which is assembled with Shimadzu Servo 4830 inside of a JEOL JSM-6510 SEM, see Fig. 2(d). All these in-situ experiments were performed under displacement control with a constant applied displacement rate of 0.02 mm/min. Detailed information of these in-situ experimental setups have been demonstrated in Fig. 2 (c) and (d).

Fig. 6. Micro damage evolution for initiation crack growth at delamination front (a) Microstructure of delamination front; (b) Initial delamination propagation.
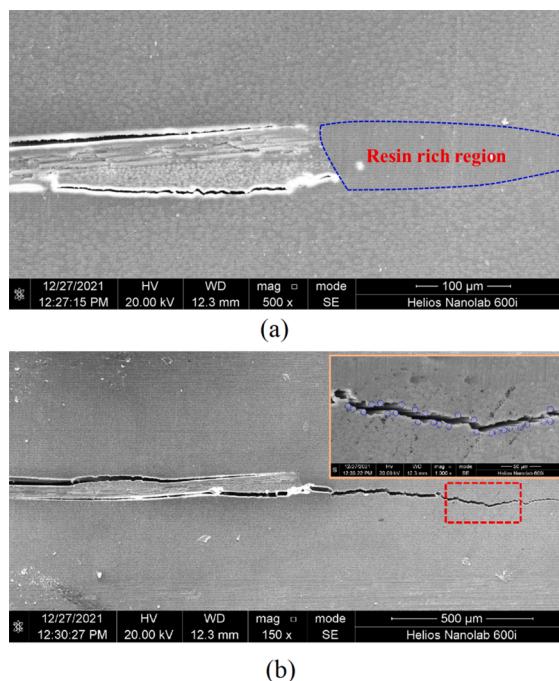
3. Interlaminar resistance and micro damage examinations

3.1. Quasi-static delamination resistance increase with fibre bridging

Three unidirectional DCB specimens, i.e. Spe-1, Spe-2 and Spe-3, were quasi-statically loaded until long enough delamination propagation, i.e. fibre bridging becomes saturation. These results are summarized in Fig. 3 in terms of interlaminar resistance G_{IC} against crack opening displacement δ. It is clear that delamination resistance can increase significantly with crack opening, and finally become plateau once crack opening exceeds a certain level.

The presence of significant bridging fibres in the wake of delamination front, as shown in Fig. 4, is the main reason for interlaminar resistance increase. Particularly, increasing bridging fibres can be present in the wake of delamination front with crack propagation. As a result, more failures can occur in these bridging fibres, which can result in more energy dissipation of a unit crack increment. However, there is an equilibrium stage, in which the amount of new bridging generation around crack front can balance with the bridging fibre final failure occurring at the end of fibre bridging region, contributing to constant interlaminar resistance with long delamination growth, as shown in Fig. 3.

Referring to the information illustrated Figs. 3 and 4, the total damage evolution in fibre-bridged crack growth can be specifically divided as: failures around crack front and in bridging fibres. It is therefore necessary to explore damage evolution related to both failures, in order to have an in-depth physical understanding on fibre-bridged delamination growth behavior. Accordingly, in-situ SEM examinations on both crack front damage evolution and fibre bridging performance were respectively conducted and discussed in what follows.

3.2. Damage mechanisms around crack front

Fig. 5 provides a typical load–displacement response of in-situ delamination tests for damage evolution observations around delamination front. There is a linear increase of the load until crack initiation. Particularly, a load drop is observed in the graph once there is delamination growth. After this falling down, the load can slightly increase until new crack propagation. And this pattern will repeat with crack opening.

SEM observations on damage evolution around delamination front were performed every 0.04 mm displacement increment during the linear response to identify if there is any initial damage occurrence. After crack initiation, SEM examinations were carried out once there is load falling down, i.e. new crack propagation.

In-situ examination results related to initiation delamination growth are summarized in Fig. 6. Particularly, Fig. 6(a) demonstrates the profile information of delamination front at the displacement of 0.200 mm (i.e. just before crack initiation) with magnification of 500X. The microstructure of pre-crack front as well as a resin rich region ahead of Teflon insert can be clearly identified. Fig. 6(b)
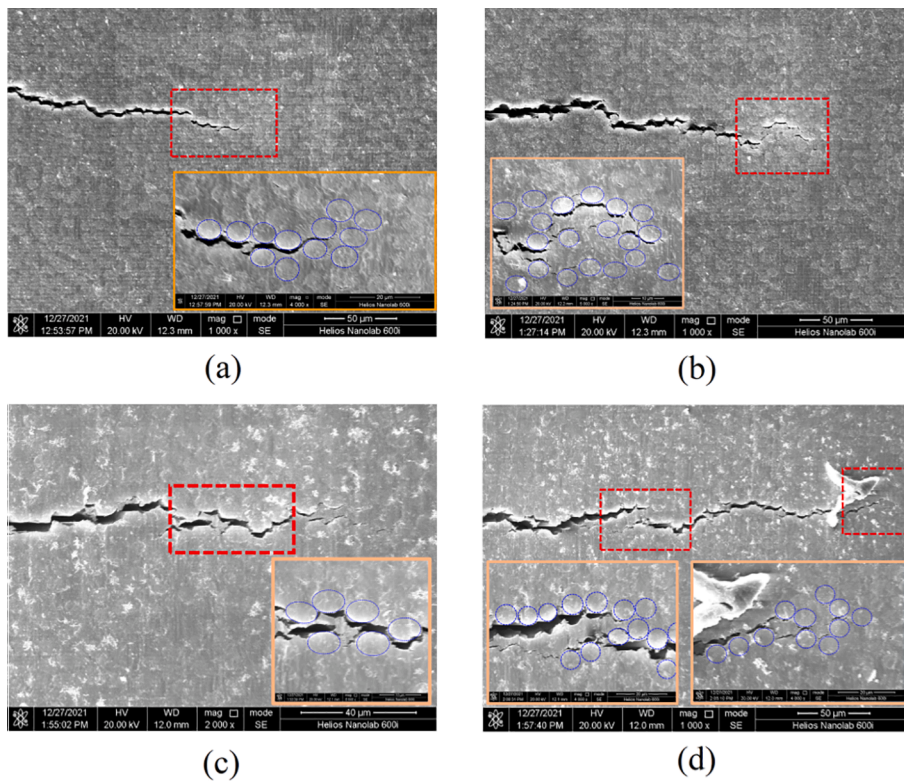
Fig. 7. Micro damage evolution for delamination growth at different displacements (a) Displacement 0.245 mm; (b) Displacement 0.260 mm; (c) Displacement 0.274 mm; (d) Displacement 0.283 mm.
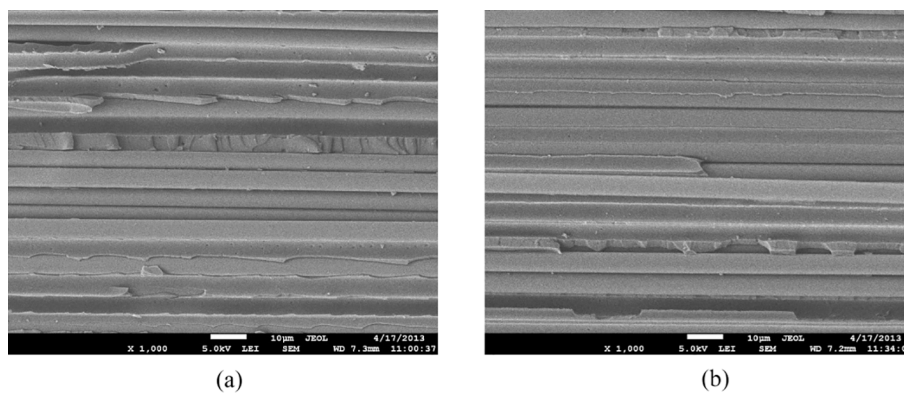

Fig. 8. SEM observation on delamination fracture surface (a) Fibre prints and hackles; (b) Dominant fibre prints on fracture surface.

provides the overall damage evolution related to initiation crack growth at the displacement of 0.235 mm (i.e. just after the initiation crack generation) with magnification of 150X. Interestingly, the initiation crack does not pass through the resin rich region, but along the boundary of this area (i.e. between fibre–matrix interface). Detailed examinations on the crack propagation path with high magnification of 1000X (at the up right corner of Fig. 6(b)) also demonstrate that crack tends to propagate along the fibre–matrix interface (the carbon fibres are marked with blue circles along the delamination path). If one takes close examinations on the crack propagation path, the surfaces of these bare carbon fibres are really smooth, without any matrix attached to the reinforcement. All this information indicates that crack resistance of the DT120 matrix is higher than that of the fibre–matrix interface. As a result, crack growth is prone to propagate along this weak interface of composite M30SC/DT120.

Fig. 7 summarizes in-situ examinations on damage evolution around delamination front after the initiation crack propagation at several displacements, i.e. 0.245 mm, 0.260 mm, 0.274 mm and 0.283 mm, with high magnification. Clear interface debonding can be identified at the delamination propagation path between reinforced carbon fibre and matrix (in which the carbon fibres are marked
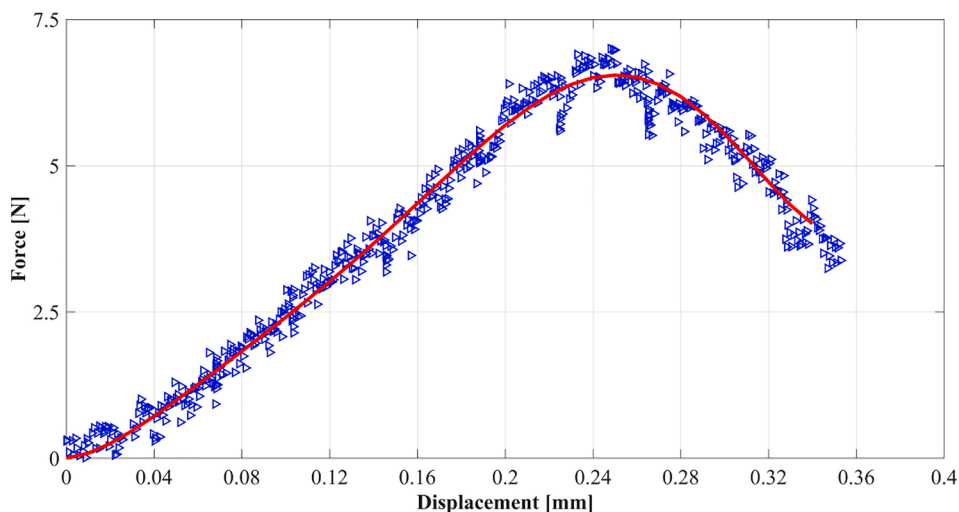
Figure 9

Fig. 9. Load-displacement response for in-situ experiments on fibre bridging.

with blue circles). Accordingly, one can conclude that fibre–matrix interface debonding is the dominant micro damage mechanism during mode I quasi-static delamination growth in composite laminates. Particularly, this interface debonding initiated at fibre–matrix interface can gradually develop and coalesce into micro-delaminations ahead of the main crack with crack opening, as shown in Fig. 7 (b), (c) and (d). The accumulation of these micro-delaminations can finally result in a macro-delamination growth (i.e. new crack generation), which will be accompanied with a sharp load falling down in the load–displacement response, as shown in Fig. 5. Repeating this pattern can contribute to continuous delamination propagation.

All above discussions on damage evolution around delamination front can provide necessary information to appropriately interpret the typical micro features observed on delamination fracture surface, i.e. fibre prints and hackles as shown in Fig. 8. It is clear that fibre–matrix interface debonding plays an important role in delamination growth, as illustrated in Figs. 6 and 7. This failure therefore can lead to fibre prints as the dominant micro feature observed on fracture surface. In addition, it should be highlighted again that the surface of the carbon fibres located on fracture surface looks really smooth (without any matrix debris attached) as shown in Fig. 8, which therefore can provide extra evidence on weak fibre–matrix interface resistance during delamination growth of composite M30SC/DT120. Hackles were observed in some locations on the fracture surface, as shown in Fig. 8. The presence of this micro feature in mode I delamination growth indeed results from local shear stress. During the micro-delamination coalescence as shown in Fig. 7, matrix between carbon fibres can be locally loaded and deformed at a shear stress state. This can lead to hackles on the fracture surfaces at some local regions. Another important reason for the appearance of hackles in mode I delamination growth is related to fibre bridging as shown in Fig. 4. Particularly, the pull-out of bridging fibres from the surrounded matrix can cause significant local shear stress, contributing to hackles on the fracture surface.

According to the above discussions, damage evolution around crack front during delamination growth can be summarized as: *Fibre-matrix interface plays an important role in determining delamination growth behavior. Initiation micro-cracks are usually present at this interface. These initial micro-cracks can gradually develop and coalesce into micro-delaminations ahead of the main crack. And the accumulation of these micro-delaminations can finally contribute to macro-delamination propagation.*

3.3. Bridging mechanisms in delamination propagation

Typical load–displacement response for in-situ samples with a certain amount of delamination propagation (i.e. a certain amount of fibre bridging) is given in Fig. 9. There is an almost linear increase of load followed by a nonlinear softening. In-situ observations on fibre bridging performance were performed at every 0.02 mm displacement increment during these tests.

In-situ examinations on the performance of bridging fibres are presented in Fig. 10. It was observed that significant bridging fibres, in terms of a single fibre or a cluster of fibres, are present at the behind of delamination front. Particularly, it was found that these bridging fibres can deform like a bending beam at the initial stage with increased displacement, see Fig. 10(a) and (b). As crack opens, these bridging fibres at the root region cannot straighten in this pattern further. As a result, fibre–matrix interface peeling/debonding can occur and propagate above the fibre root, see Fig. 10(c) and (d). In the last stage, fibre breakage can be observed at the root region due to high bending stress, see Fig. 10(e) and (f).

Fractographic examinations on delamination fracture surface were carried out to provide extra evidence on the bridging mechanisms during delamination growth. Obvious fibre failure can be identified on the delamination fracture surface, as shown in Fig. 11(a). Fig. 11(b) provides a local observation of Fig. 11(a) with high magnification of 1000X. Both matrix spalling resulted from fibre-matrix peeling/debonding and damaged carbon fibres can be identified. These observed features are indeed in line with the in-situ SEM
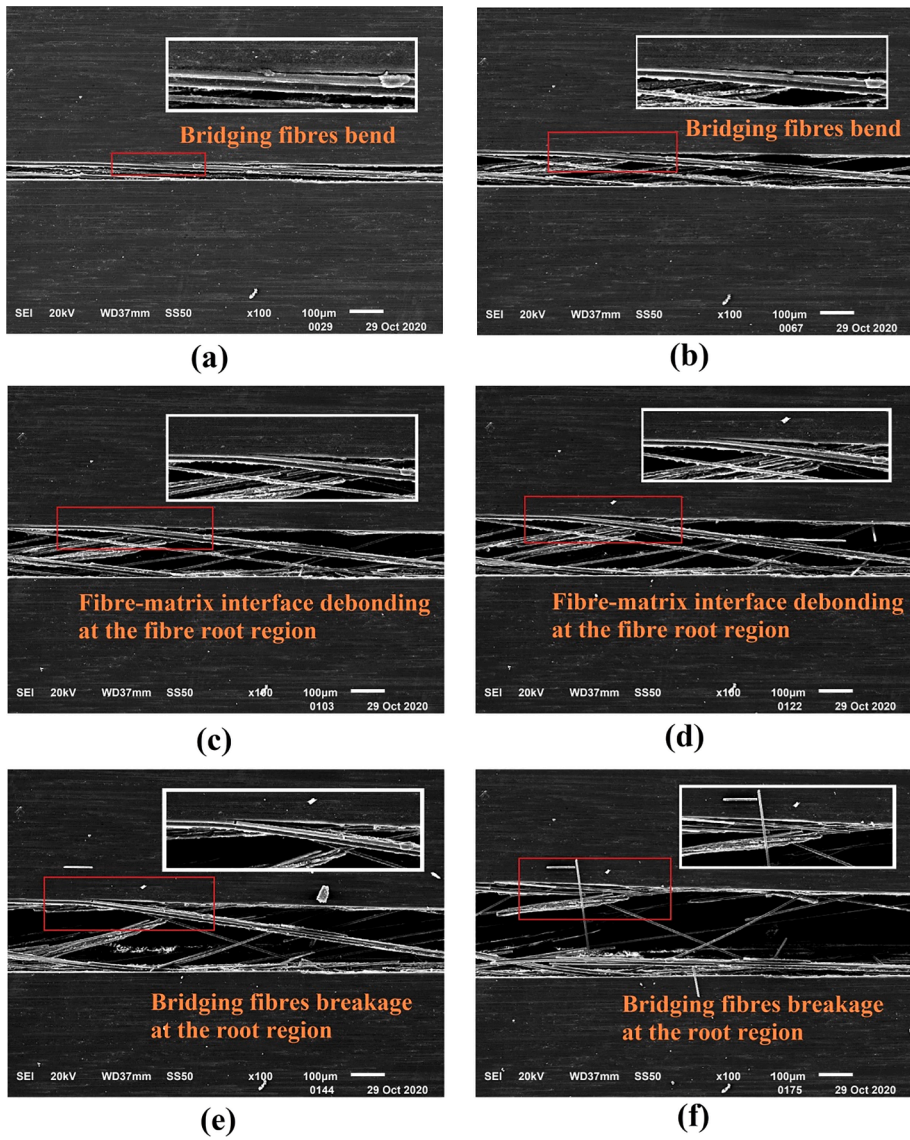
Fig. 10. Damage evolution in bridging fibres at different displacements (a) Displacement 0.04 mm; (b) Displacement 0.12 mm; (c) Displacement 0.20 mm; (d) Displacement 0.24 mm; (e) Displacement 0.28 mm; (f) Displacement 0.34 mm.
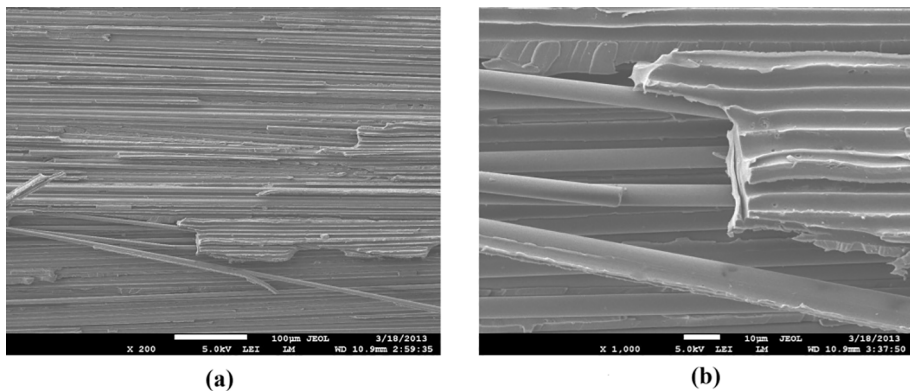

Fig. 11. SEM examinations on delamination fracture surface (a) Overall SEM examinations; (b) Local SEM examinations.
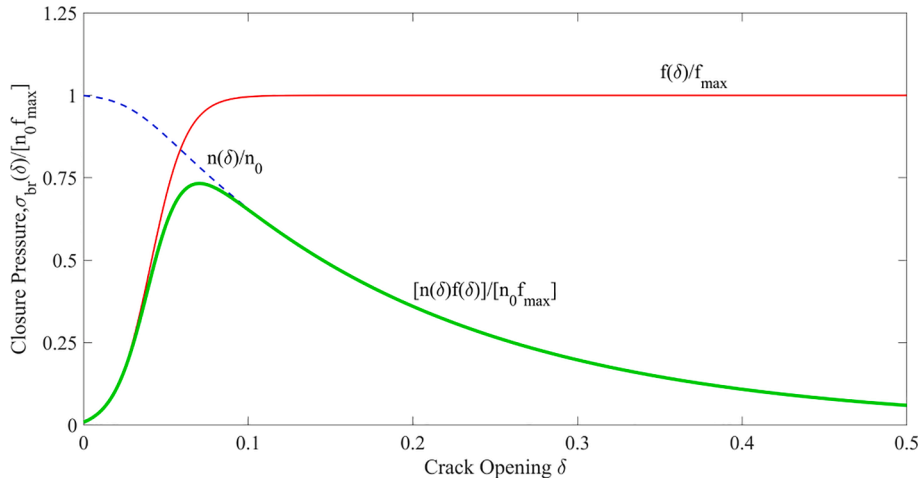
Fig. 12. Bridging stress distribution theoretical analysis.

Table 1
Parameters for bridging stress theoretical analysis [26].

n_0	$\delta*$ [mm]	d [mm]	l_0 [mm]	E [GPa]	K_{IC}^{matrix} [MPa·mm$^{0.5}$]	α
30	0.03	0.02	0.41	193	22.14	0.40
φ_{max}	l_{ref} [mm]	σ_{ref} [MPa]	$\overline{\sigma}_b$ [MPa]	τ [MPa]	C_b	m
11.00	25.00	1630	6000	5.00	0.5	3.1

characterizations on the performance of bridging fibres as illustrated in Fig. 10.

According to these in-situ SEM examinations and fractographic results illustrated in Figs. 10 and 11, fibre bridging mechanisms in mode I quasi-static delamination growth of carbon fibre reinforced composite laminates can be summarized as: *Bridging fibres first bend like a short beam and contribute to significant tensile loads. Fibre-matrix crack propagation subsequently occurs at the root, and releases the tensile loads with increased crack opening. Fibre breakage can occur at the root in the final stage, causing bridging stress decrease with further crack opening.*

According to above discussions on bridging mechanisms, a micromechanical model proposed in literature [26] was employed here to evaluate the real bridging stress distribution during delamination growth in composites. This model will be briefly introduced here. People who have further interests are referred to literature [26].

In principle, bridging closure stress depends on both the force applied on per fibre $f(\delta)$ and the number of bridging fibres at per unit area $n(\delta)$ [26]. Accordingly, the bridging closure stress $\sigma_{br}(\delta)$ can be evaluated via Eq.(3).

$$\sigma_{br}(\delta) = f(\delta) \cdot n(\delta) \tag{3}$$

Referring to the bridging mechanisms reported in the present study, bridging fibres in the first stage (as shown in Fig. 10(a) and (b)) can bear significant tensile forces and have great contribution to sharp of bridging stress increase. The force of per fibre in this stage can be determined using the knowledge of fibre bending deformation with crack opening. However, the magnitude of $f(\delta)$ can be limited with matrix spalling in the second stage. With a combination of these two stages, bridging stress before reaching its maximum can be determined via Eq.(4) [26]. Particularly, the first part of the right-hand side represents closure stress derived from tensile stress in bridging fibre, which provides great contribution to the crack closure stress. The second part represents bridging stress resulted from fibre bending. The sum of these two parts can contribute to bridging closure stress, which can increase significantly with crack opening. And the occurrence of matrix spalling observed above the fibre root (as shown in Fig. 10(c) and (d)) can lead to a steady state in the crack-closing-force of a fibre.

$$\sigma_{br}(\delta) = n_0 \left[\frac{3\pi}{64} \frac{Ed^4}{l_0^2} \left(\frac{\delta}{l_0} \right) + \frac{\pi d^2}{4} \sqrt{\frac{2\tau El_0}{d}} \left(\frac{\delta}{l_0} \right)^2 \right] \tag{4}$$

where n_0 is the initial number of bridging fibres at per unit area, which can be assumed to be constant until a reference crack opening $\delta*$; d is the fibre diameter; l_0 is the initial bridging length; E is the fibre modulus.

In the last stage, the number of bridging fibres at per unit area can decrease with crack opening. This number is assumed to obey the Weibull distribution [26]. Accordingly, the bridging closure stress in this stage (as shown in Fig. 10(e) and (f)) can be evaluated via Eq. (5) [26].
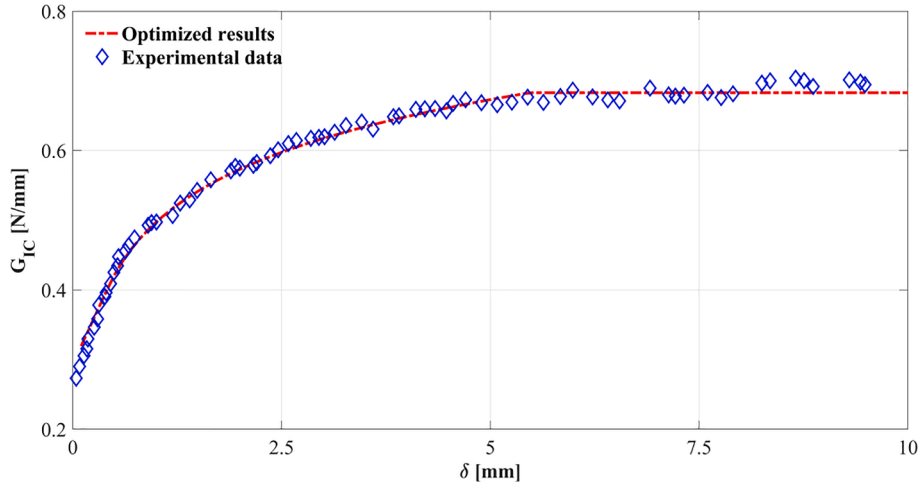
Fig. 13. Comparison of G_{IC} vs δ.

$$\sigma_{br}(\delta) = \alpha\sqrt{\pi}n_0 K_{IC}^{matrix} a^{3/2} \times \exp\left[-\frac{C_b}{\sin\varphi_{\max} \cdot l_{ref}}\left(\frac{\overline{\sigma}_b}{\sigma_{ref}}\right)^m (\delta - \delta^*)\right] \tag{5}$$

where K_{IC}^{matrix} represents mode I fracture toughness of the matrix; α is the ratio of crack propagation length along and perpendicular to the fibre; φ_{max} is the bridging angle at the plateau state; l_{ref} and σ_{ref} are reference constants; $\overline{\sigma}_b$ represents the average value of the maximum stress applied at the root of the fibre; and m is the Weibull modulus.

Based on the bridging mechanisms identified in Fig. 10, a representative shape of the bridging closure stress calculated via Eqs.(3) to (5) with the parameters provided in literature [26] are given in Fig. 12. Table 1 gives a summary of these parameters used in bridging closure stress analysis. It is clear that the bridging stress can significantly increase with crack opening, and becomes soften once crack opening is approaching to a certain level. After this, the bridging closure stress can nonlinearly decrease with further crack opening.

According to above discussion on bridging mechanisms as well as the shape of bridging stress distribution, a trapezoid-nonlinear softening law Eq.(6) was proposed to capture the essential feature of the bridging closure stress distribution.

$$\sigma_{br}(\delta) = \begin{cases} K\delta & \left(\delta \leq \dfrac{\sigma_{c1}}{K}\right) \\ \sigma_{c1} & \left(\dfrac{\sigma_{c1}}{K} < \delta \leq \delta_{c1}\right) \\ \dfrac{\sigma_{c1}\delta_{c1}}{\delta} & \left(\delta_{c1} < \delta \leq \delta_{f1}\right) \\ 0 & \left(\delta_{f1} < \delta\right) \end{cases} \tag{6}$$

where σ_{c1} represents the peak bridging stress; δ_{c1} is the crack opening at the end of plateau; and δ_{f1} represents the crack opening at which bridging stress becomes zero. These parameters can be determined via an optimization algorithm programmed in MATLAB with the experimentally determined R-curve data shown in Fig. 3.

Taking the results of Spe-1 as an example, Fig. 13 provides an evidence of using this trapezoid-nonlinear relation Eq.(6) in the determination of delamination resistance via J-integral Eq.(7). It is clear that the use of this new traction-separation law can appropriately determine bridging contribution to interlaminar resistance increase in fibre-bridged delamination growth. To the authors' opinion, the reason for this accurate description of delamination resistance increase is closely associated with physical understanding on both bridging mechanisms and the explicit shape of bridging stress distribution. As a result, an appropriate traction-separation relation Eq.(6) can be derived to accurately determine the bridging performance during delamination growth of composite laminates.

$$G_{IC}(\delta) = G_0 + G_{br} = G_0 + \int_0^{\delta_{f1}} \sigma_{br}(\delta)d\delta \tag{7}$$

4. FEA model for fibre-bridged delamination growth simulation

4.1. New cohesive constitutive for delamination with fibre bridging

Damage evolution in both crack front and bridging fibres should be appropriately represented for fibre-bridged delamination growth characterization. Referring to the superposition strategy proposed by Davila et al [28], a new delamination constitutive can be
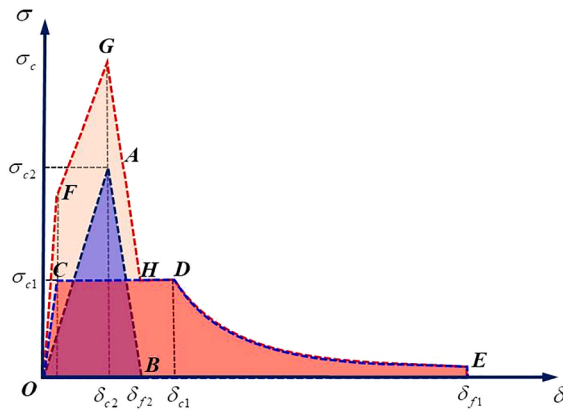
Fig. 14. Schematic of the fibre-bridged delamination constitutive via superposition strategy.
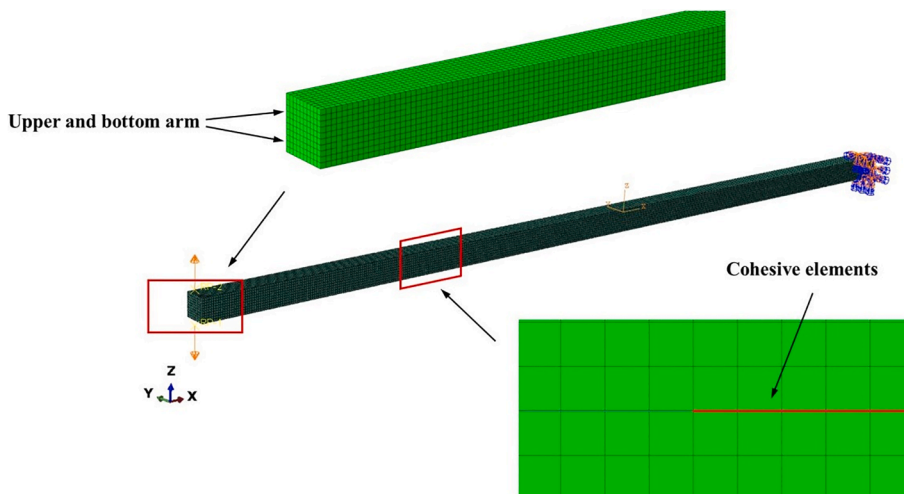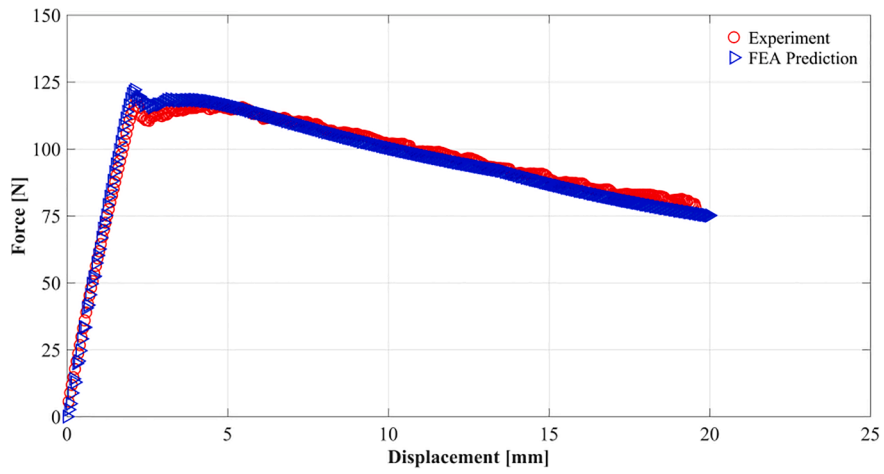

Fig. 15. FEA delamination model.

Table 2
Dimensions and delamination constitutive parameters.

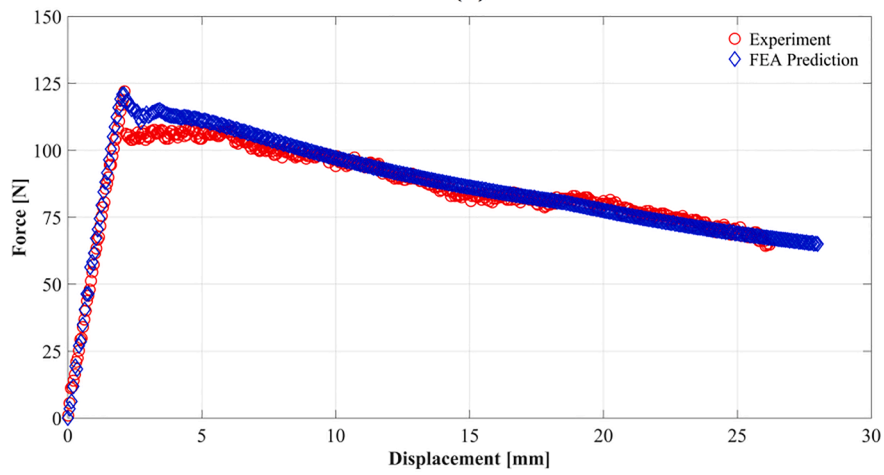|	Length [mm]	Width [mm]	Thickness [mm]	a_0 [mm]	G_0 [J/m²]	σ_{c1} [MPa]	σ_{c2} [MPa]	δ_{c1} [mm]	δ_{f1} [mm]
Spe-1	200	25.1	5.0	43.5	291.2	0.26	24.0	0.41	5.50
Spe-2	200	25.3	5.0	43.5	291.2	0.17	24.0	0.65	9.03
Spe-3	200	24.7	5.0	43.5	291.2	0.21	24.0	0.72	6.57

proposed to represent fibre-bridged delamination behavior, as schematically illustrated in Fig. 14. Particularly, a bilinear softening law, i.e. *OAB* with a high peak stress σ_{c2} and a short critical opening displacement δ_{f2}, is used to represent damage evolution around crack front. And a trapezoid-nonlinear softening relation, i.e. *OCDE* with a low strength σ_{c1} but a long critical opening displacement δ_{f1}, is employed to represent fibre bridging performance. Eventually, a new delamination constitutive, i.e. *OFGHDE*, can be superposed to determine the total damage evolution in fibre-bridged delamination growth in composites.

4.2. FEA numerical simulations of delamination in composite M30SC/DT120

Delamination growth in DCB specimens were simulated via 3D finite element meshes to verify the validation of the proposed new delamination constitutive. Particularly, a total number of 64,000 8-node solid elements (C3D8R) were prepared to discretize the DCB arms. A thin layer (0.01 mm) of 8-node three-dimensional cohesive elements (COH3D8) with the number of 3130 was located between the arms to simulate delamination propagation. The new fibre-bridged delamination constitutive, as schematically illustrated in Fig. 14, was implemented in these cohesive elements via programming the ABAQUS user subroutine VUMAT. To increase the
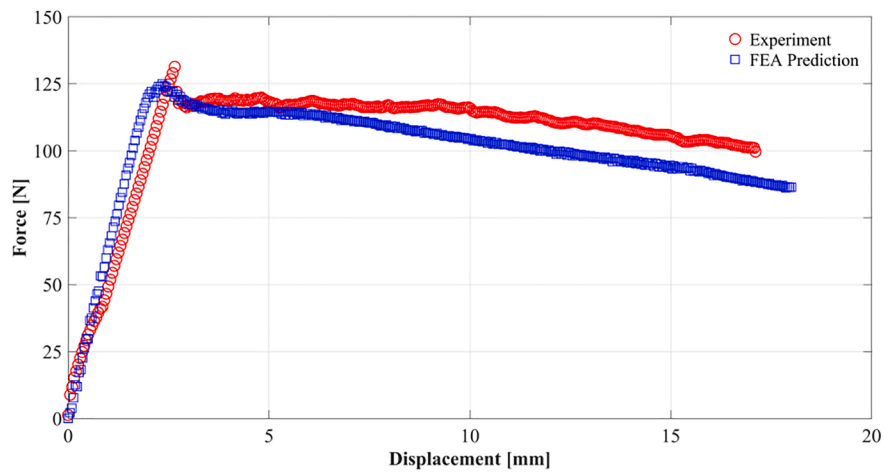
Fig. 16. Fibre-bridged delamination predictions of M30SC/DT120 composites (a) Spe-1; (b) Spe-2; (c) Spe-3.

Table 3
Specimen dimensions and delamination constitutive parameters.

	Length [mm]	Width [mm]	Thickness [mm]	a_0 [mm]	G_0 [J/m^2]	σ_{c1} [MPa]	σ_{c2} [MPa]	δ_{c1} [mm]	δ_{f1} [mm]
[30]	180	25.0	4.16	35.0	100.0	1.97	15.0	0.063	10.32
[31]	280	25.2	4.0	60.0	270.0	0.11	20.0	0.379	10.64
[32]	150	25.0	4.5	35.0	131.3	1.65	15.0	0.057	10.32

computation efficiency, only one fifth of each DCB specimen along the width direction was discretized and simulated.

Detailed information of the FEA model is illustrated in Fig. 15. The material properties of M30SC/DT120 composite laminates are referred to literature [29]. Dimension information and delamination constitutive parameters are summarized in Table 2.

Fig. 16 provides a comparison on all experimental and numerical load–displacement results. These results clearly demonstrate that the FEA predictions can agree well with the experiments from crack initiation to really long delamination propagation. Accordingly, one can make a conclusion that the proposed constitutive model can accurately characterize fibre-bridged delamination growth behavior in composites. Furthermore, this good agreement highlights the importance of exploring bridging mechanisms, as well as using an appropriate traction-separation relation to well represent bridging performance in delamination growth study.

4.3. Model validation via experimental data from literatures

All above simulations can provide the first evidence on the validation of using this proposed delamination model in representing fibre-bridged delamination behavior in carbon fibre reinforced composites. In order to have extra evidence on the effectiveness of this model, it was used to predict delamination growth behavior with fibre bridging reported in literatures [30–32]. Table 3 summarizes the DCB specimen dimensions and delamination constitutive parameters used in these numerical simulations.

All the results obtained from the FEA simulations and the experimental data are compared in Fig. 17. As expected, the prediction results can agree well with the experimental data during the entire delamination growth, i.e. from crack initiation to long propagation. As a result, one can make a conclusion again that the proposed constitutive model, as schematically illustrated in Fig. 14, can well account for fibre bridging in delamination simulations of composites.

The reason for the success of using this new delamination constitutive in determining delamination growth behavior with fibre bridging is closely associated with the physical interpretations on fibre bridging mechanisms. According to these in-situ examinations on bridging mechanisms, the real bridging stress distributed in bridging fibres can be well discussed and identified via the micromechanical model [26]. As a result, one can propose a traction-separation relation to appropriately capture the essential feature of bridging stress distribution, rather than use an arbitrary bridging law without physical background to phenomenologically represent bridging performance in the perspective energy balance. To the author's opinion, this research pattern is really important for future study on developing appropriate traction-separation relation in representing different bridging performance.

5. Concluding remarks

Micro damage mechanisms for delamination growth in carbon fibre reinforced composites with fibre bridging have been thoroughly explored via in-situ SEM observations and fractographic analysis in the present study. Particularly, the total damage evolution in fibre-bridged delamination growth can be specifically divided into failures around crack front and in bridging fibres. Damage evolution around delamination front can be characterized as: Initial micro-cracks occur at fibre–matrix interface. These initial micro-cracks can gradually develop and coalesce into micro-delaminations ahead of the main crack. The accumulation of these micro-delaminations can finally cause macro delamination growth. In-situ SEM examinations on fibre bridging demonstrated that bridging fibres can experience bending, fibre–matrix peeling and final breakage with crack opening. According to these identified bridging mechanisms, the micromechanical model proposed in literature [26] was applied to explore the real shape of bridging stress distribution. It was found that bridging closure stress can significantly increase to a peak with crack opening. After this, bridging stress can experience a nonlinear softening.

A new delamination constitutive, appropriately capturing the essential feature of bridging stress distribution, has been proposed to determine fibre-bridged delamination behavior via superposing a bilinear cohesive law representing damage evolution around crack front, with a trapezoid-nonlinear traction-separation relation representing fibre bridging performance. This new delamination constitutive was implemented into the cohesive zone formulation via programming ABAQUS user subroutine. It was found that the use of this new delamination constitutive model can well determine fibre-bridged delamination behavior from crack initiation to long crack propagation of different composites, demonstrating the effectiveness of using this new model in fibre-bridged delamination growth characterization.

This study highlights the importance of having physical understanding on fibre-bridged delamination behavior for developing a reliable prediction model. Particularly, the shape of bridging stress distribution can be well identified via the micromechanical model [26] in accordance with the in-situ investigations on bridging mechanisms. Thus, an appropriate traction-separation relation with physical interpretations can be proposed to represent fibre bridging performance. And a new delamination constitutive model can be finally developed to accurately determine fibre-bridged delamination growth behavior in composites.
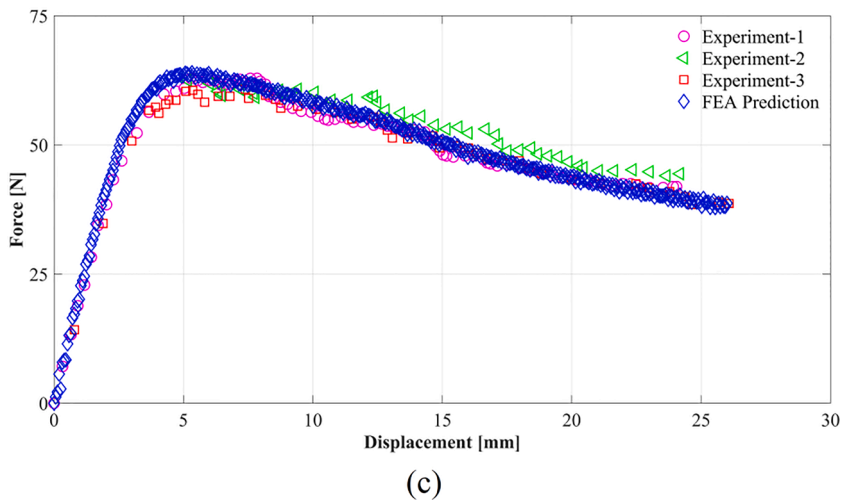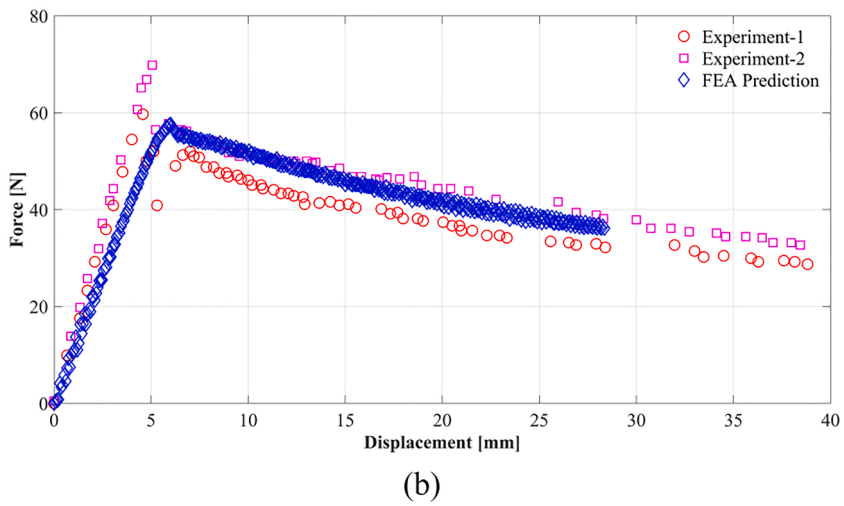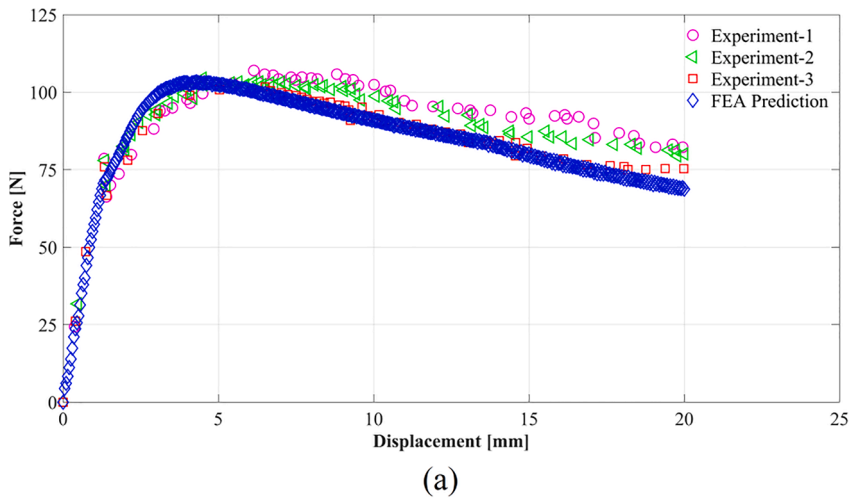
Fig. 17. Fibre-bridged delamination predictions for composites reported in literature (a) Literature [30]; (b) Literature [31]; (c) Literature [32].

CRediT authorship contribution statement

Liaojun Yao: Writing – review & editing, Writing – original draft, Visualization, Validation, Supervision, Software, Resources, Project administration, Methodology, Investigation, Funding acquisition, Formal analysis, Data curation, Conceptualization. **Jurui Liu:** Visualization, Validation, Software, Methodology, Formal analysis, Data curation. **Zhangming Lyu:** Software, Formal analysis, Data curation. **R.C. Alderliesten:** . **Cui Hao:** . **Chuanxi Ren:** Resources, Investigation. **Licheng Guo:** Resources, Methodology.

Declaration of Competing Interest

The authors declare that they have no known competing financial interests or personal relationships that could have appeared to influence the work reported in this paper.

Data availability

Data will be made available on request.

Acknowledgements

References

[1] Pascoe JA, Alderliesten RC, Benedictus R. Methods for the prediction of fatigue delamination growth in composites and adhesive bonds - A critical review. Engng Fract Mech 2013;112–113:72–96.

[2] Bak BLV, Sarrado C, Turon A, Costa J. Delamination under fatigue loads in composite laminates: A review on the observed phenomenology and computational methods. Appl Mech Rev 2014;66:060803.

[3] Yao L, Cui H, Guo L, Sun Y. A novel total fatigue life model for delamination growth in composite laminates under generic loading. Compos Struct 2021;258:113402.

[4] Heidari-Rarani M, Sayedain M. Finite element modeling strategies for 2D and 3D delamination propagation in composite DCB specimen using VCCT, CZM and XFEM approaches. Theor Appl Fract Mech 2019;103:102246.

[5] Sorensen BF, Jacobsen TK. Large-scale bridging in composites: R-curves and bridging laws. Compos A Appl Sci Manuf 1998;29:1443–51.

[6] Jensen SM, Bak BLV, Bender JJ, Carreras L, Lindgaard E. Transient delamination growth in GFRP laminates with fibre bridging under variable amplitude loading in G-control. Compos B Engng 2021;225:109296.

[7] Yao L, Alderliesten R, Zhao M, Benedictus R. Bridging effect on mode I fatigue delamination behavior in composite laminates. Compos A Appl Sci Manuf 2014;63:103–9.

[8] Yao L, Cui H, Sun Y, Guo L, Chen X, Zhao M, et al. Fibre-bridged fatigue delamination in multidirectional composite laminates. Compos A Appl Sci Manuf 2018;115:175–86.

[9] Ghadirdokht A, Heidari-Rarani M. Delamination R-curve behavior of cured composite laminates. Compos B Engng 2019;175:107139.

[10] Khan R. Fiber bridging in composite laminates: A literature review. Compos Struct 2019;229:111418.

[11] Farmand-Ashtiani E, Cugnoni J, Botsis J. Specimen thickness dependence of large scale fiber bridging in mode I interlaminar fracture of carbon epoxy composite. Int J Solids Struct 2015;55:58–65.

[12] Farmand-Ashtiani E, Alanis D, Cugnoni J, Botsis J. Delamination in cross-ply laminates: Identification of traction-separation relations and cohesive zone modelling. Compos Sci Technol 2015;119:85–92.

[13] Daneshjoo Z, Shokrieh MM, Fakoor M. A micromechanical model for prediction of mixed-mode I/II delamination of laminated of composites considering fiber bridging effects. Theor Appl Fract Mech 2018;94:46–56.

[14] Liu W, Chen P. Determination of the bridging law for mixed-mode I/II delamination without measuring the crack length and crack relative displacements. Theor Appl Fract Mech 2020;109:102750.

[15] Suo Z, Bao G, Fan B. Determination R-curve phenomena due to damage. J Mech Phys Solids 1992;40:1–16.

[16] Jacobsen TK, Sorensen BF. Mode I intra-laminar crack growth in composites-modelling of R-curves from measured bridging laws. Compos A Appl Sci Manuf 2001;32:1–11.

[17] Donough MJ, Gunnion AJ, Orifici AC, Wang CH. Scaling parameter for fatigue delamination growth in composites under varying load ratios. Compos Sci Technol 2015;120:39–48.

[18] Tamuzs V, Tarasovs S, Vilks U. Progressive delamination and fiber bridging modeling in double cantilever beam composite specimens. Engng Fract Mech 2001;68:513–25.

[19] Shokrieh MM, Salamat-talab M, Heidari-Rarani M. Effects of initial crack length on the measured bridging law of unidirectional E-glass/epoxy double cantilever beam specimens. Mater Des 2014;55:605–11.

[20] Gong Y, Chen X, Li W, Zhao L, Tao J, Zhang J, et al. Delamination in carbon fiber epoxy DCB laminates with different stacking sequences: R-curve behavior and bridging traction-separation relation. Compos Struct 2021;262:113605.

[21] Fernberg SP, Berglund LA. Bridging law and toughness characterisation of CSM and SMC composites. Compos Sci Technol 2001;61:2445–54.

[22] Stutz S, Cugnoni J, Botsis J. Crack-fiber sensor interaction and characterization of the bridging tractions in mode I delamination. Engng Fract Mech 2011;78:890–900.

[23] Stutz S, Cugnoni J, Botsis J. Studies of mode I delamination in monotonic and fatigue loading using FBG wavelength multiplexing and numerical analysis. Compos Sci Technol 2011;71:443–9.

[24] Spearing SM, Evans AG. The role of fiber bridging in the delamination resistance of fiber-reinforced composites. Acta Metall Mater 1992;40:2191–9.

[25] Bao G, Suo Z. Remarks on crack-bridging concepts. Appl Mech Rev 1992;45:355–66.

[26] Kaute DAW, Shercliff HR, Ashby MF. Delamination, fibre bridging and toughness of ceramic matrix composites. Acta Metall Mater 1993;41:1959–70.

[27] Mortell DJ, Tanner DA, McCarthy CT. In-situ SEM study of transverse cracking and delamination in laminated composite materials. Compos Sci Technol 2014;105:118–26.

[28] Davila CG, Rose CA, Camanho PP. A procedure for superposing linear cohesive laws to represent multiple damage mechanisms in the fracture of composites. Int J Fract 2009;158:211–23.

[29] R. Rodi. The residual strength failure sequence in fiber metal laminates. PhD Thesis. 2012, TU Delft.

[30] Yin S, Gong Y, Li W, Zhao L, Zhang J, Hu N. A novel four-linear cohesive law for the delamination simulation in composite DCB laminates. Compos B Engng 2020;180:107526.

[31] Blondeau C, Pappas G, Botsis J. Influence of ply-angle on fracture in antisymmetric interfaces of CFRP laminates. Compos Struct 2019;216:464–76.

[32] Shokrieh MM, Salamat-talab M, Heidari-Rarani M. Dependency of bridging traction of DCB composite specimen on interface fiber angle. Theor Appl Fract Mech 2017;90:22–32.